JBC RESEARCH ARTICLE

The synaptic scaffolding protein CNKSR2 interacts with CYTH2 to mediate hippocampal granule cell development

Received for publication, April 30, 2021, and in revised form, November 2, 2021 Published, Papers in Press, November 17, 2021,
https://doi.org/10.1016/j.jbc.2021.101427

Hidenori Ito[1,*], **Rika Morishita**[1], **Mariko Noda**[1], **Tomoki Ishiguro**[1], **Masashi Nishikawa**[1], **and Koh-ichi Nagata**[1,2,*]

From the [1]*Department of Molecular Neurobiology, Institute for Developmental Research, Aichi Developmental Disability Center, Kasugai, Aichi, Japan;* [2]*Department of Neurochemistry, Nagoya University Graduate School of Medicine, Showa-ku, Nagoya, Japan*

Edited by Paul Fraser

CNKSR2 is a synaptic scaffolding molecule that is encoded by the *CNKSR2* gene located on the X chromosome. Heterozygous mutations to *CNKSR2* in humans are associated with intellectual disability and epileptic seizures, yet the cellular and molecular roles for CNKSR2 in nervous system development and disease remain poorly characterized. Here, we identify a molecular complex comprising CNKSR2 and the guanine nucleotide exchange factor (GEF) for ARF small GTPases, CYTH2, that is necessary for the proper development of granule neurons in the mouse hippocampus. Notably, we show that CYTH2 binding prevents proteasomal degradation of CNKSR2. Furthermore, to explore the functional significance of coexpression of CNKSR2 and CYTH2 in the soma of granule cells within the hippocampal dentate gyrus, we transduced mouse granule cell precursors *in vivo* with small hairpin RNAs (shRNAs) to silence CNKSR2 or CYTH2 expression. We found that such manipulations resulted in the abnormal localization of transduced cells at the boundary between the granule cell layer and the hilus. In both cases, CNKSR2-knockdown and CYTH2-knockdown cells exhibited characteristics of immature granule cells, consistent with their putative roles in neuron differentiation. Taken together, our results demonstrate that CNKSR2 and its molecular interaction partner CYTH2 are necessary for the proper development of dentate granule cells within the hippocampus through a mechanism that involves the stabilization of a complex comprising these proteins.

In humans, neurodevelopmental disorders present with a spectrum of diverse phenotypic characteristics such as intellectual disability (ID), cognitive deficits, learning and memory deficits, anxiety, and difficulties with social interaction (1). For ID syndromes such as Fragile X syndrome, Rett syndrome, and Down syndrome, phenotypic traits arise from genetic abnormalities that disrupt the development of multiple regions of the brain, including the hippocampus (2). Comprising the *cornu ammonis* (hippocampus proper) and the dentate gyrus, separated by the hippocampal sulcus, this brain region is critical for learning and memory. Of note, the development of the hippocampus commences prenatally but concludes postnatally, as evidenced by the finding that up to 85% of dentate granule neurons are born after birth in mice (3).

Presently, the molecular mechanisms of hippocampal neurogenesis and the impact of genetic mutations on these important developmental events in the mammalian brain remain to be better characterized. For example, the X chromosome contains genes associated with cognitive function, including *FMR1* (4, 5) and *NLGN3* (6). Indeed, mutations in either of these genes lead to ID and autism (7–10), yet numerous other genes remain poorly characterized, despite clinical genetic evidence implicating their essential functions in brain development and disease (11, 12). One such gene is *CNKSR2*, associated with ID and epilepsy (13–19).

CNKSR2 [connector enhancer of KSR-2, also known as MAGUIN (membrane-associated guanylate kinase-interacting protein)] was initially identified as a binding partner for PSD (postsynaptic density)-95 and S-SCAM (synaptic scaffolding molecule) (20, 21). CNKRS2's expression is enriched in the brain, including the hippocampus (20). Additionally, many CNKSR2 mutations have been found in individuals with ID and epilepsy (13–19), yet its functions in human neurons are poorly understood. The gene encodes a 1034 amino acid polypeptide that functions as a scaffold protein, containing multiple domains such as a SAM (sterile alpha motif) domain, a CRIC (conserved region in CNK) domain, a PDZ domain, a PH (pleckstrin homology) domain, and a C-terminal PDZ-binding motif (20, 21). Notably, the internal proline-rich motif interacts with ARHGAP39/Vilse, a Rac GTPase-activating protein (GAP), to influence hippocampal neuron spine morphogenesis (22). Also, the C-terminal coiled-coil region of CNKSR2 binds to CYTH2/Cytohesin2/ARNO (22), a guanine nucleotide exchange factor (GEF) for ARF small GTPases, to induce Rac activation (23). Furthermore, CNKSR2 also interacts with ARHGEF7, a Rac-specific GEF, to influence Rac signaling within cells (22). Additionally, CNKSR2 interacts with Ras small GTPase effectors, Raf and Rlf (21), and participates in the NGF (nerve growth factor)-dependent ERK (extracellular signal-regulated kinase) activation in PC12 cells (24). Thus, CNKSR2 is involved in various intracellular

* For correspondence: Hidenori Ito, itohide@inst-hsc.jp; Koh-ichi Nagata, knagata@inst-hsc.jp.

© 2021 THE AUTHORS. Published by Elsevier Inc on behalf of American Society for Biochemistry and Molecular Biology. This is an open access article under the CC BY license (http://creativecommons.org/licenses/by/4.0/).

signaling pathways combined with different molecular partners, with relevance to signaling in neural cells.

In this study, we investigated the role of CNKSR2 in the development of cells of the hippocampus. Using an electroporation-based *in vivo* gene transfer method, which we established previously (25), We report that CNKSR2 interacts with its binding partner, CYTH2, to stabilize protein levels within cells. Also, suppression of CNKSR2 or CYTH2 influences the localization and differentiation of neonatally born dentate granule cells during mouse brain development. Thus, disruptions to CNKSR2 and CYTH2 in cells may disrupt the formation of dentate granule cells to cause hippocampal dysfunction in mammals.

Results

CNKSR2 forms a complex with CYTH2 or ARHGAP39 and is stabilized by them

Previous reports identify CNKSR2 as a mediator of Rac signaling (22) through its interactions with other proteins, including ARHGAP39, CYTH2, and ARHGEF7. Thus, we began by exploring the interaction between CNKSR2 and these proteins. As shown, immunoprecipitation experiments using lysates from transiently transfected COS7 cells revealed that CNKSR2 interacted with ARHGAP39 and CYTH2, but not with ARHGEF7 under the experimental conditions (Fig. 1*A*). Interestingly, these results also suggested that the presence of CYTH2 and ARHGAP39 led to an increase in immunodetectable CNKSR2 signal (Fig. 1*A*). To investigate this possibility, we repeated our experiments. We found that cotransfection of CNKSR2 with CYTH2, ARHGAP39, but not ARHGEF7 or GFP, led to increased CNKSR2 immunoblot signal in cell lysates (Fig. 1, *B* and *C*). Notably, cotransfection of CYTH2 led to the most pronounced increase in immunoblotted CNKSR2 signal. Guided by this insight, we explored the effects of exogenously derived CYTH2 on CNKSR2 levels in the presence of the protein synthesis inhibitor cycloheximide. Figure 2, *A*–*C* shows western blot and quantitative analyses of lysates following time course treatment with cycloheximide. In this experiment, we loaded reduced amounts of protein extracted from CYTH2-transfected cells to avoid the saturation of the signal. The calculated half-life of exogenously derived CNKSR2 with cotransfected CYTH2 is significantly higher than when coexpressed with GFP (Fig. 2*C*). This suggests that CYTH2 influences the stability of CNKSR2. We further investigated this possibility by testing the effects of MG132, a proteasome inhibitor, on CYTH2-induced CNKSR2 protein stabilization. Figure 2, *D* and *E* show that MG132 significantly increased immunoblotted for exogenously derived CNKSR2 cotransfected with GFP or CYTH2. However, we observed that while the magnitude of difference in intensity of immunoblotted CNKSR2 signal in the presence of the unrelated GFP protein was approximately 4.0-fold, the magnitude of difference in intensity of CNKSR2 signal in the presence of CYTH2 was only 1.6-fold (Fig. 2*E*). We interpret this result to indicate that the capacity for CNKSR2 to be targeted for ubiquitin-proteasome-mediated protein degradation is influenced by the presence of CYTH2 but not the unrelated GFP protein.

Expression analyses of CNKSR2 in mouse brain

To investigate endogenous CNKSR2 protein, we produced a specific antibody, which we confirm by the following analysis. First, we performed western blotting on lysates from cells transduced with a myc-CNKSR2 expression construct together with a control (nontargeting) shRNA vector or with a CNKSR2 targeting shRNA vector. As shown, immunoblotted myc-CNKSR2 signals that accord with the molecular size of approximately 130 kDa (indicated with an asterisk) are visible using our anti-CNKSR2 antibody and anti-myc antibody, but these respective signals are significantly diminished in lysates of cells cotransfected with shCNKSR2 (Fig. S1*A*). Second, following validation of our antibody, we performed western blotting on whole-brain extracts of mice from postnatal (P) days 0 to 30. Consistent with the molecular weights for signals validated in our specificity testing (Fig. S1*A*), CNKSR2 immunoblotted signal of about 110 kDa was faintly detected at P0 and was more intense by P7–P30, while a 130 kDa signal was weakly detected until P15 through to P30 (Fig. 3*A*). We also investigated the expression of CYTH2 and detected two immunoblots of approximately 50 kDa that were prominent from P0 to P30 and a lower-molecular-weight band that was detected from P0 to P15 (Fig. 3*A*). These bands may be isoforms or products of posttranslational modification such as phosphorylation (26–29). Further analyses should be required to address this issue. In order to substantiate their protein–protein interaction *in vivo*, we found that endogenous CYTH2 protein, which corresponds to the upper band, could be immunoprecipitated from protein lysates extracted from mouse cerebral cortices and hippocampal tissues with our anti-CNKSR2 antibody (Fig. 3*B*). In addition, given the specificity of our anti-CNKSR2 antibody (Fig. S1*C*), we performed immunohistochemical analyses using sections of a P7 mouse brain to find prominent CNKSR2 signal in the soma of pyramidal cells within the *cornu ammonis*, as well as in granule cells of the dentate gyrus (Fig. 3*C*, *a*–*d*). Parallel studies with an anti-CYTH2 antibody enabled us to visualize cytosolic staining in pyramidal and dentate granule cells (Fig. 3*C*, *e*–*h*).

CNKSR2 and CYTH2 control the neonatal development of dentate granule cells

Given the expression of CNKSR2 and CYTH2 in the developing P7 hippocampus (Fig. 3*C*), we investigated the roles of these two factors in the development of dentate granule cells in neonatal mice. To achieve this, we used an electroporation-based *in vivo* gene transfer method, which we previously established (25). This method is highly effective for the analysis of hippocampal cell differentiation and maturation. We previously took this approach to clarify the functions of the small GTPases, Rac1, Rac3, and Cdc42, and their roles in the localization and differentiation of dentate granule cells (30). Our approach enables us to study neonatally born dentate neurons and their migration and terminal differentiation

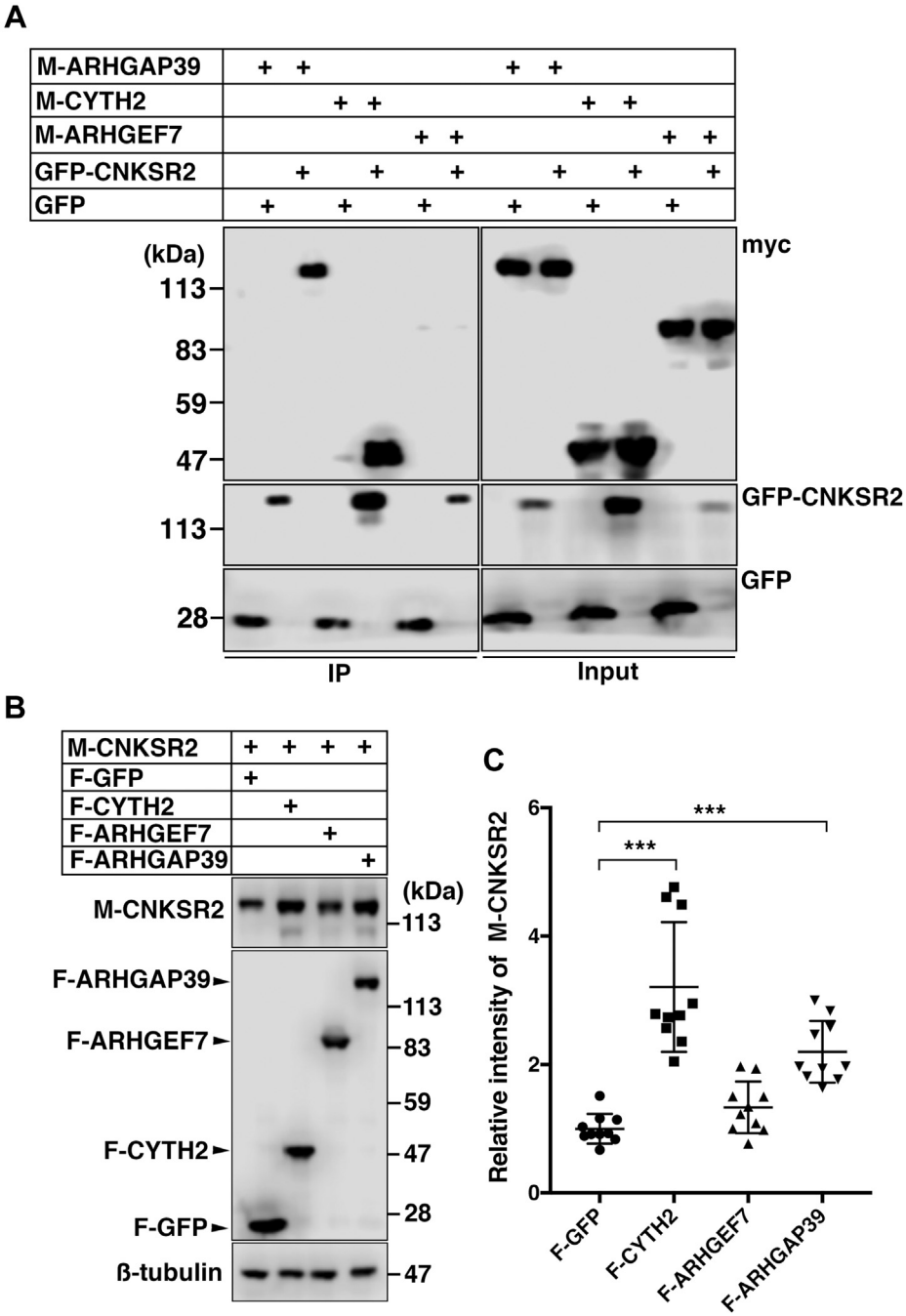

Figure 1. Stabilization of CNKSR2 through the interaction with CYTH2 and ARHGAP39. *A*, interaction of CNKSR2 with CYTH2 and ARHGAP39. COS7 cells were transfected with pCAG-GFP or pCAG-GFP-CNKSR2 together with pCAG-myc-ARHGAP39, -myc-CYTH2 or, -myc-ARHGEF7. After 48 h, cells were harvested with IP buffer, followed by immunoprecipitation with anti-GFP. Immunoprecipitates (IP) and lysates (Input) were subjected to western blotting using anti-myc (*upper panel*) and anti-GFP (*middle* and *lower panels*). Molecular size markers appear at the *left*. *B*, effect of CYTH2, ARHGEF7, or ARHGAP39 on the expression level of CNKSR2. COS7 cells were transfected with pCAG-myc-CNKSR2 together with pCAG-Flag-GFP, pCAG-Flag-CYTH2, pCAG-Flag-ARHGEF7, or pCAG-Flag-ARHGAP39. After 48 h, cells were harvested with lysis buffer and cell lysates (10 μg of protein) were subjected to western blotting using anti-myc (*upper panel*) and anti-Flag (*middle panel*). β-tubulin was shown as the loading control (*lower panel*). Molecular size markers appear at the *right*. *C*, quantification of the expression of myc-CNKSR2. Immunoreactive bands shown in *B* were quantified and graphed. The signals of myc-CNKSR2 were normalized to β-tubulin. Each bar shows the mean ± SD from ten dishes. ***$p < 0.001$.

(Fig. 4*A* and see Experimental procedures for further details) (25). Specifically, we investigated the consequences of suppression of CNKSR2 using two shRNA targeting vectors (shCNKSR2#1 and shCNKSR2#2) on the development of P0 dentate granule cells. We began by validating their capacity for knockdown of exogenously derived myc-CNKSR2 in transiently transfected COS7 cells. As shown, both shCNKSR2#1 and shCNKSR2#2, but not a nontargeting control shCont vector, efficiently suppressed immunodetectable myc-CNKSR2 signal (Fig. 4*Ba*). We also confirmed that these targeting shRNA vectors could suppress endogenous CNKSR2 in mouse neuroblastoma cell line Neuro2a cells (Fig. S1*B*).

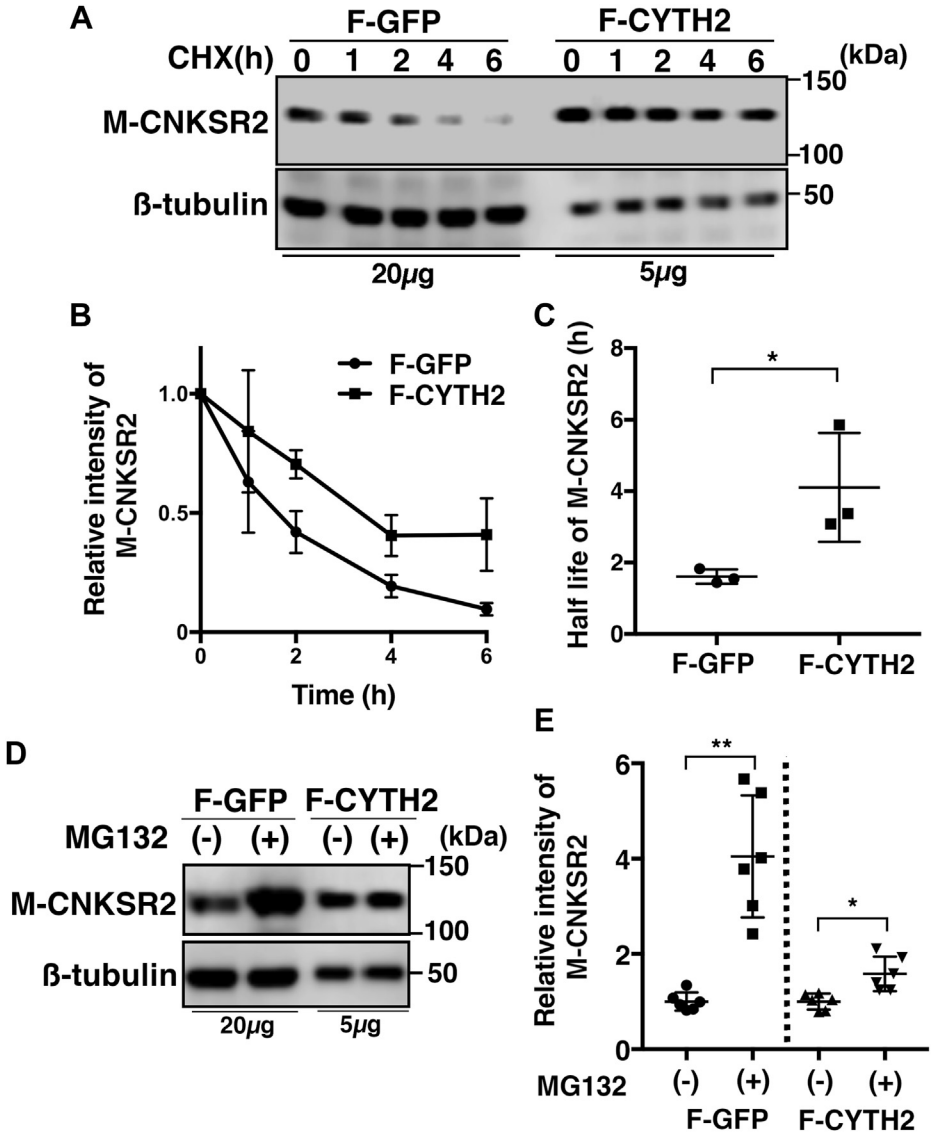

Figure 2. CYTH2 protects CNKSR2 from proteasome-mediated degradation. *A*, cycloheximide chase assay. COS7 cells were cotransfected with pCAG-myc-CNKSR2 together with pCAG-Flag-GFP or pCAG-Flag-CYTH2. After 48 h, cells were incubated with cycloheximide (300 μg/ml) for the indicated times before processing. Cell lysates (20 μg of protein for GFP-expressing cells and 5 μg for CYTH2-expressing cells) were subjected to western blotting using anti-myc. β-tubulin was shown as the loading control. Molecular size markers appear at the *right*. *B*, bands in *A* were quantified and graphed. Each bar shows the mean ± SD from three dishes. *C*, the half-life of CNKSR2 was calculated and graphed. Each bar shows the mean ± SD from three experiments. *$p < 0.05$. *D*, effects of MG132 on the expression of CNKSR2. COS7 cells were transfected with as in *A*. After 32 h, cells were incubated with MG132 (5 μM) for 16 h. Cell lysates (20 μg and 5 μg of protein for GFP- and CYTH2-expressing cells, respectively) were then prepared and subjected to western blotting using anti-myc. Molecular size markers appear at the *right*. *E*, bands in *D* were quantified and graphed. Each bar shows the mean ± SD from six dishes. **$p < 0.01$, *$p < 0.05$.

Next, we coelectroporated a GFP-expression vector (pCAG-GFP) with shCNKSR2#1, shCNKSR2#2, or shCont into neonatal dentate granule precursors by *in vivo* electroporation in P0 brains, after which mice were allowed to recover before processing for analysis at P21 (25). As shown, in the control treatment, in which cells were transduced with GFP and nontargeting (shCont) shRNA vector, GFP-positive cells were predominantly located within the granule cell layer (GCL), as deduced by quantifying labeled cells within the GCL, GCL/hilus junction and the hilus (Fig. 4*B*, *b* and *e*). In contrast, cells transfected with shCNKSR2#1 or #2 were frequently mislocalized at the GCL/hilus region or hilus (Fig. 4*B*, *c–e*). Furthermore, the mislocalization of dentate neurons following shCNKSR2 knockdown could be ameliorated by cotransfection with an expression construct for CNKSR2 that is resistant to shRNA-mediate knockdown (Fig. S2). Therefore, this result indicates that CNKSR2 is necessary and sufficient to influence the positioning of P0-born granule cells within the postnatal P21 hippocampus. To account for the possibility that knockdown affects the viability of electroporated cells, we quantified GFP-labeled cells in the dentate gyrus to find that the absolute numbers of labeled cells were not significantly different between the treatment of targeting shRNAs or nontargeting control vector (Fig. 4, *Bf*).

Given that CYTH2 interacts with CNKSR2 in granule cells *in vivo* to form a stable complex, we investigated the impact of

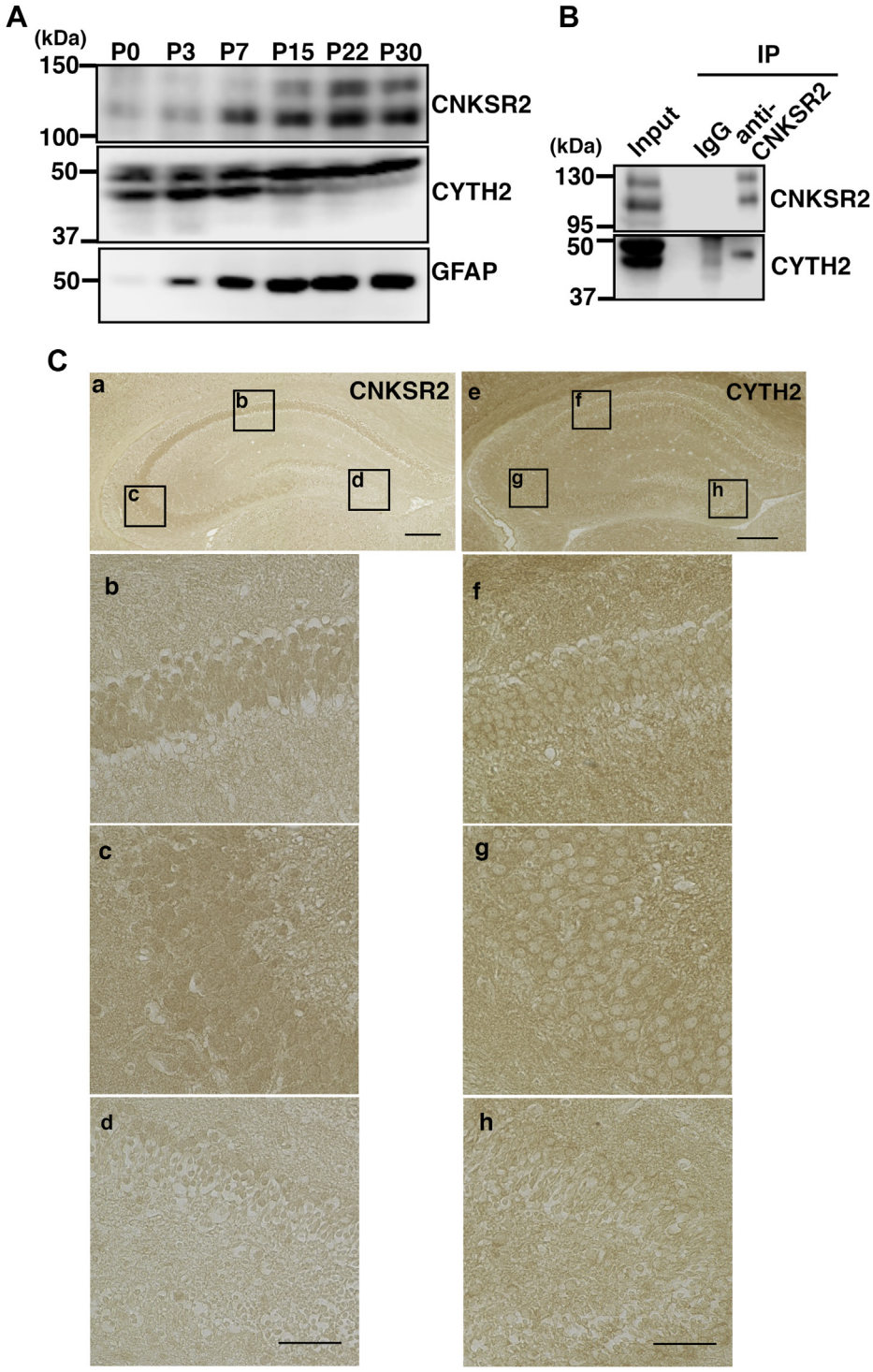

Figure 3. Characterization of CNKSR2 and CYTH2 in mouse brain. *A*, developmental expression of CNKSR2 and CYTH2 immunoblotted protein signals. Whole-brain extracts (30 μg of proteins for CNKSR2 and CYTH2, and 5 μg for GFAP) were subjected to SDS-PAGE followed by western blotting with anti-CNKSR2 (*upper panel*) and anti-CYTH2 (*middle panel*). GFAP is shown as a marker of brain tissue differentiation (*bottom panel*). Molecular size markers appear at the *left*. *B*, complex formation of CNKSR2 and CYTH2 in mouse brain. Lysates were incubated with rabbit IgG or anti-CNKSR2. Immunoprecipitates were subjected to western blotting with anti-CNKSR2 (*upper panel*) or anti-CYTH2 (*lower panel*). Molecular weight markers appear at the *left*. *C*, immunohistochemical analyses of CNKSR2 and CYTH2 in the hippocampus. Sections of the hippocampus prepared at P7 were stained with anti-CNKSR2 (*a–d*) or anti-CYTH2 (*e–h*). Images were obtained using BZ-9000 microscope. Boxed areas in *a* and *e* were magnified in *b–d* and *f–h*, respectively. Scale bars, 200 μm (*a* and *e*) and 50 μm (*d* and *h*).

CYTH2 shRNA-mediated knockdown using a similar approach in P0-born granule cells. We designed two shRNA vectors targeting unique sequences, namely shCYTH2#1 and #2, that could efficiently knockdown steady-state levels of CYTH2 protein in transiently transfected cells (Fig. 4*Ca*). Following *in vivo* electroporation of neonatal dentate granule

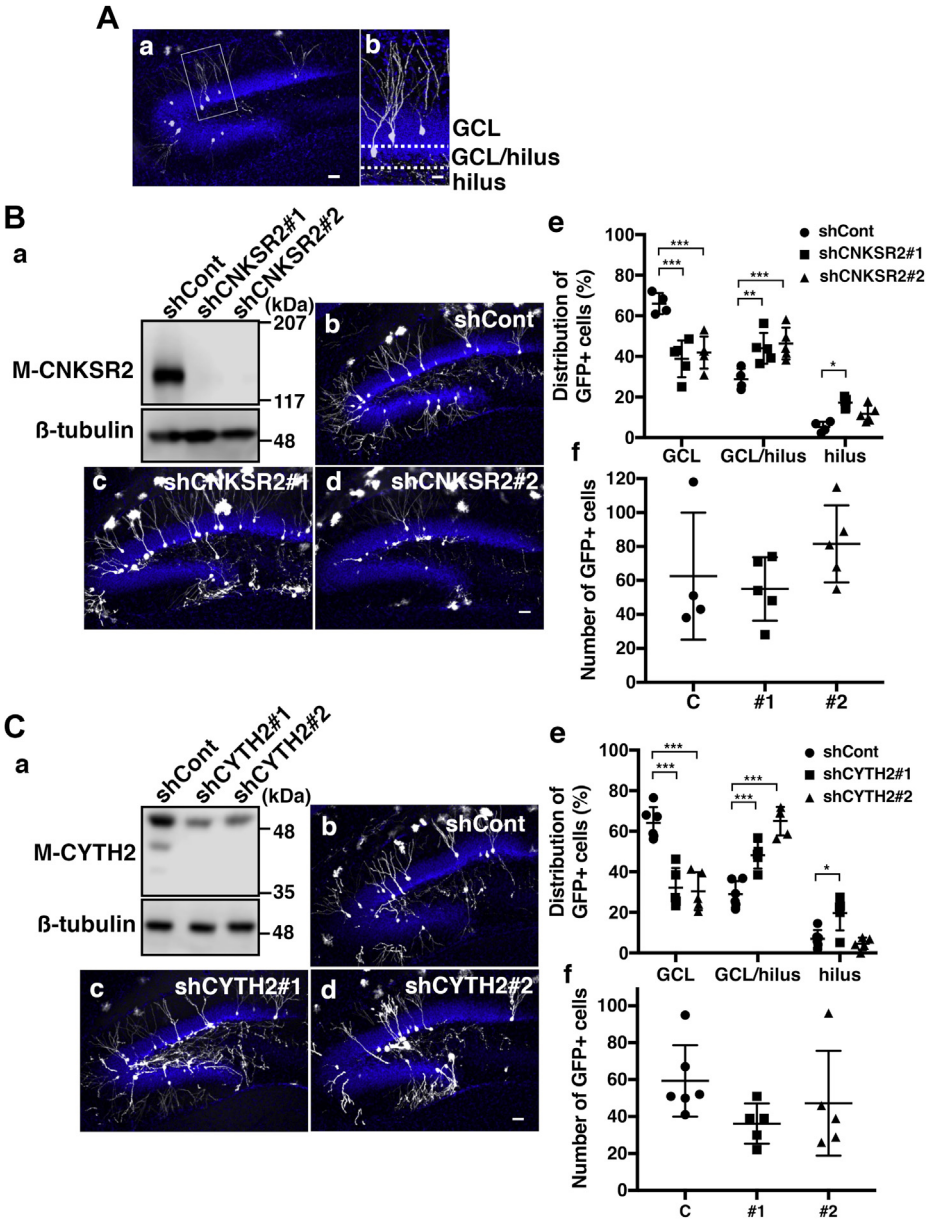

Figure 4. Effects of knockdown of CNKSR2 and CYTH2 on the localization of neonatally born dentate granule cells. *A*, the definition of the region in the dentate gyrus. The dentate gyrus was divided into granule cell layer (GCL), border zone of GCL and hilus (GCL/hilus), or hilus as indicated. *B*, effects of knockdown of CNKSR2 (*a*) Characterization of knockdown vectors for CNKSR2. COS7 cells were transfected with pCAG-myc-CNKSR2 together with shCont, shCNKSR2#1 or #2. After 48 h, cells were collected and subjected to western blot analysis using anti-myc. β-tubulin was shown as the loading control. Molecular weight markers appear at the *right*. (*b–d*) Localization of control (*b*) and CNKSR2-deficient (*c* and *d*) cells. pCAG-GFP was coelectroporated with shCont (*b*), shCNKSR2#1 (*c*), or #2 (*d*) into the lateral ventricle of P0 mice. After 21 days, sections were prepared and stained with anti-GFP (*white*). Nuclei were stained with DAPI (*blue*). Scale bar, 50 μm. *e*, quantitation of the localization. GFP-positive cells in GCL, GCL/hilus, or hilus were counted and graphed. The data were shown as the percentage of GFP-positive cells in the individual parts of the dentate gyrus. Each bar shows the mean ± SD. shCont, n = 4; shCNKSR2#1, n = 5; shCNKSR2#2, n = 5. ***$p < 0.001$, **$p < 0.01$, *$p < 0.05$. *f*, the absolute cell number in the dentate gyrus. GFP-positive cells counted in *e* were graphed. Each bar shows the mean ± SD. shCont, n = 4; shCNKSR2#1, n = 5; shCNKSR2#1, n = 5; *C*, effects of knockdown of CYTH2. *a*, characterization of knockdown vectors for CYTH2. COS7 cells were transfected with pCAG-myc-CYTH2 together with shCont, shCYTH2#1 or #2. Western blot analyses were performed as in *B, a*. Molecular weight markers appear at the *right*. (*b–d*) Localization of control (*b*) and CYTH2-deficient (*c* and *d*) neonatally born cells. pCAG-GFP was coelectroporated with shCont (*b*), shCYTH2#1 (*c*), and #2 (*d*) into the lateral ventricle of P0 mice. Analyses were carried out as in *B, b–d*. Scale bar, 50 μm. *e*, quantitation of the localization. Analyses were performed as in *B, e*. shCont, n = 6; shCYTH2#1, n = 5; shCYTH2#2, n = 5. ***$p < 0.001$, *$p < 0.05$. *f*, the absolute cell number in the dentate gyrus. GFP-positive cells counted in *e* were graphed. Each bar shows the mean ± SD. shCont, n = 6: shCYTH2#1, n = 5; shCYTH2#2, n = 5. The image of *A, b* was captured by FV1000 confocal microscope and the others were obtained using BZ-9000 microscope.

precursors in the P0 hippocampus with shCYTH2#1 or #2, in conjunction with the GFP-expression construct (pCAG-GFP) to label cells, we observed that shCYTH2-treated cells were abnormally localized to the GCL/hilus border or hilus in a distribution that was significantly different to control-treated (GFP and shCont) cells (Fig. 4*C*, *b–e*). This effect of shCYTH2 knockdown in granule cell positioning within the dentate gyrus is reminiscent of the effect of shCNKSR2 knockdown. We quantified GFP-labeled cells between treatments to find that the absolute number of labeled cells was not

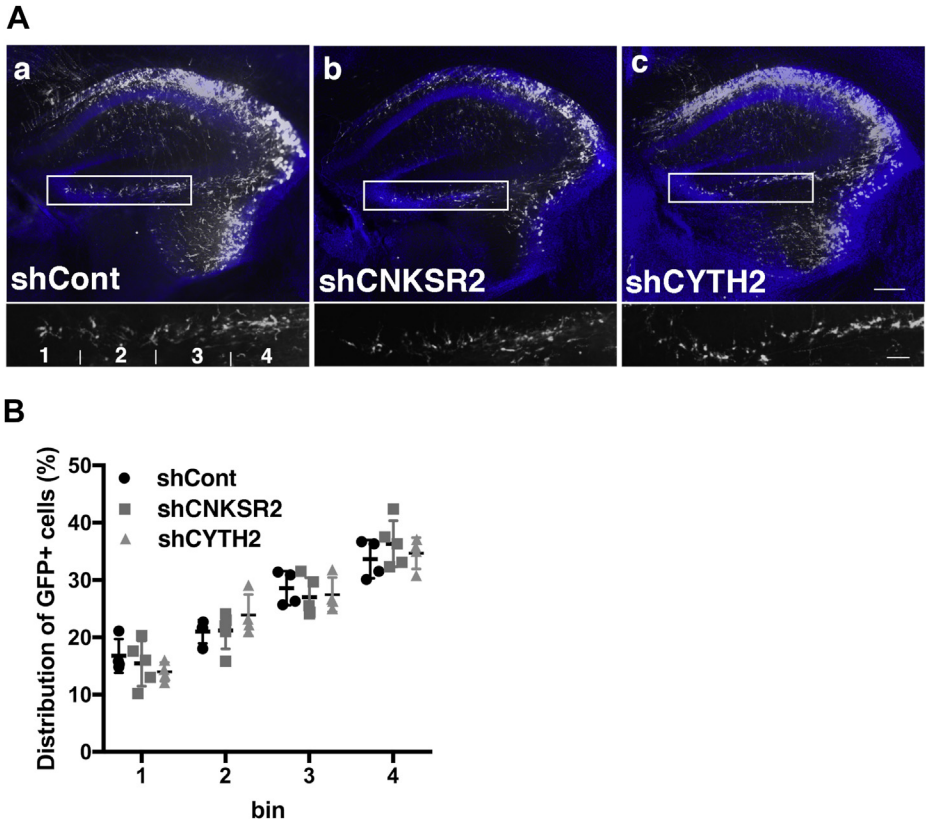

Figure 5. Effects of knockdown of CNKSR2 and CYTH2 on the migration at early postnatal age of neonatally born dentate granule cells. *A*, *a–c*, analyses of cell positioning of granule cells at the early postnatal stage. After mice were electroporated at P0, coronal sections were prepared at P4 and stained for GFP (*green*) and DAPI (*blue*). Squared regions in *upper panels* were magnified in *lower panels*. Images were obtained using BZ-9000 microscope. Scale bars, 200 μm (*upper panel*) and 100 μm (*lower panel*). *B*, relative fluorescence intensity in each bin was quantified and graphed. Each bar shows mean ± SD. shCont, n = 4; shCNKSR2#1, n = 5; shCYTH2, n = 4.

significantly different across shRNA treatments, indicating that knockdown with CYTH2-targeting shRNAs did not influence cell viability (Fig. 4*Cf*).

While the positioning of P0-born granule cells within the hippocampus at P21 was significantly influenced by knockdown with shCNKSR2 and shCYTH2 targeting vectors compared with control treatment, their mispositioning was unclear and represented a delay or a defect in migration. To test this, we performed electroporation and then analyzed coronal sections of treated brains at P4, analyzing the distribution of transfected cells within the stream of migration, as described. As shown in Figure 5, *A* and *B*, we observed that the distribution of GFP-labeled cells was not significantly different across shRNA treatments. Therefore, this result suggests that the mislocalization of P0-born granule cells within hippocampus at P21 may be explained by the fine-tuning of granule cell positioning within the GCL after P4 in the mouse.

Given that the terminal differentiation of GCL cells is critical to their cellular functions, we next analyzed the effects of CNKSR2 and CYTH2 knockdown on treated cells that coexpress GFP. In the control (shCont) treatment, labeled cells exhibited a polarized shape with dendrites projecting to the molecular layer (Fig. 6*A*), a finding consistent with previous reports (25, 30). In contrast, however, cells transduced with shCNKSR2 and shCYTH2 vectors showed features consistent with a loss of neuronal polarity and abnormal neurite morphology (Fig. 6, *A–C*). Moreover, this abnormal morphology appeared to be more severe with shCNKSR2-treated cells (Fig. 6, *B* and *C*).

Next, we examined the effects of the knockdown of ARHGAP39 on the localization of P0-born granule cells. We did this because ARHGAP39 is a binding partner for CNKSR2, and the presence of ARHGAP39 could enhance CNKSR2 levels, based on our biochemical studies (see Fig. 1*B*). As shown in Figure S3, treatment with two unique shARHGAP39 vectors did not significantly change the placement of labeled cells in the GCL/hilus or hilus. However, treatment with shARHGAP39#1 significantly increased the proportion of labeled cells within the GCL.

The differentiation of neonatally born dentate granule cells is influenced by knockdown of CNKSR2 and CYTH2 expression in vivo

During their development, dentate granule cells express stage-specific differentiation markers, including Prox1, which defines postmitotic dentate granule cells, and NeuN in immature and mature neurons and calbindin, detected in mature neurons dentate granule cells (31). We performed immunostaining for these markers on sections of brains transduced with nontargeting (shCont), shCNKSR2, or shCYTH2 vectors to examine potential effects of knockdown

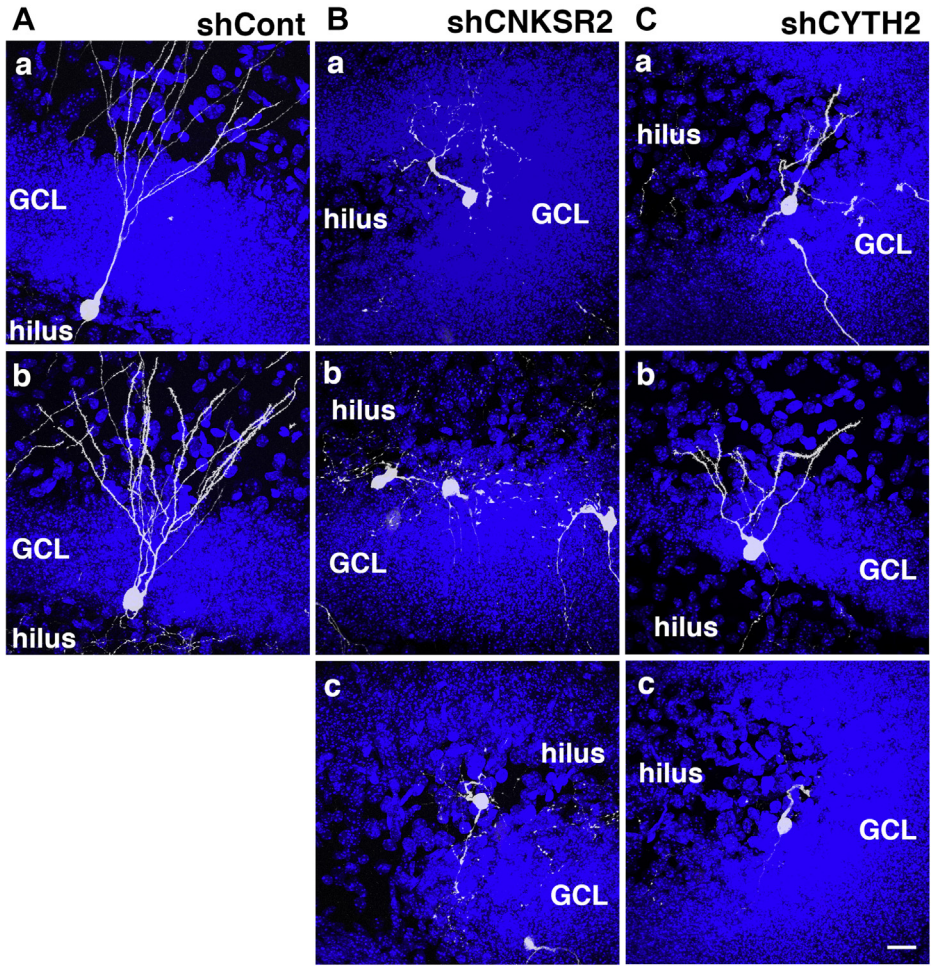

Figure 6. Morphological change of the CNKSR2-or CYTH2-deficient mislocalized cells. After electroporation at P0, coronal brain sections were prepared at P21. Sections were stained with anti-GFP (*white*) and DAPI (*blue*). Images were captured with FV1000 confocal microscope and z-stacked images of dentate neurons localized at the GCL/hilus region were shown. Scale bar, 20 μm.

on these cellular features. We found that for cells located within the GCL, the immunostaining signals for Prox1, NeuN, and calbindin were not significantly different in intensity, irrespective of treatment with control (shCont), shCNKSR2, or shCYTH2 vectors (data not shown). In contrast, however, when we examined immunostaining of these markers for cells localized to the GCL/hilus boundary or within the hilus, we observed a significant effect with CNKSR2 and CYTH2 knockdown, as follows: Figure 7, *A* and *B* shows that compared with control (shCont) treatment, treatment with shCNKSR2 and shCYTH2 knockdown vectors led to a significant decrease in the intensity of Prox1 immunostaining signal within cells, with a more severe effect observed for shCYTH2-treated cells. These results suggest that the knockdown of either gene has affected the maturation of these granule cells. We also quantified the signal for NeuN to observe a significant decrease in cells transduced with shCNKSR2 and shCYTH2 knockdown vectors (Fig. 7, *C* and *D*). In the case of calbindin, a marker of mature granule neurons, we found that knockdown with shCNKSR2 or shCYTH2 shRNAs led to a decrease in signal shCNKSR2 treatment leading to a more severe effect. Taken together, the expression of CNKSR2 and CYTH2 is essential to the development of granule cells of the mouse hippocampus.

Discussion

In this study, we have investigated the biological significance of CNKSR2 and its binding partners within cells and their putative roles in developing neonatally born dentate granule cells in mice. We found that its binding partners CYTH2 and ARHGAP39 can influence steady-state levels of exogenously derived CNKSR2 in transfected cells. Notably, the synthesis and ubiquitin-proteasome-mediated turnover of CNKSR2 are influenced by CYTH2 *in vitro*, and their protein–protein interaction is relevant to cells of the mouse brain *in vivo*. Furthermore, we found that suppression of CNKSR2 or CYTH2 expression influences the development of P0-born granule cells of the P21 hippocampus in different ways. Previous studies have described functions for CNKSR2 in dendritic development and spine formation in primary cultured neurons *in vitro* (22). However, our current study represents the first report of CNKSR2 function in developing hippocampal cells *in vivo*.

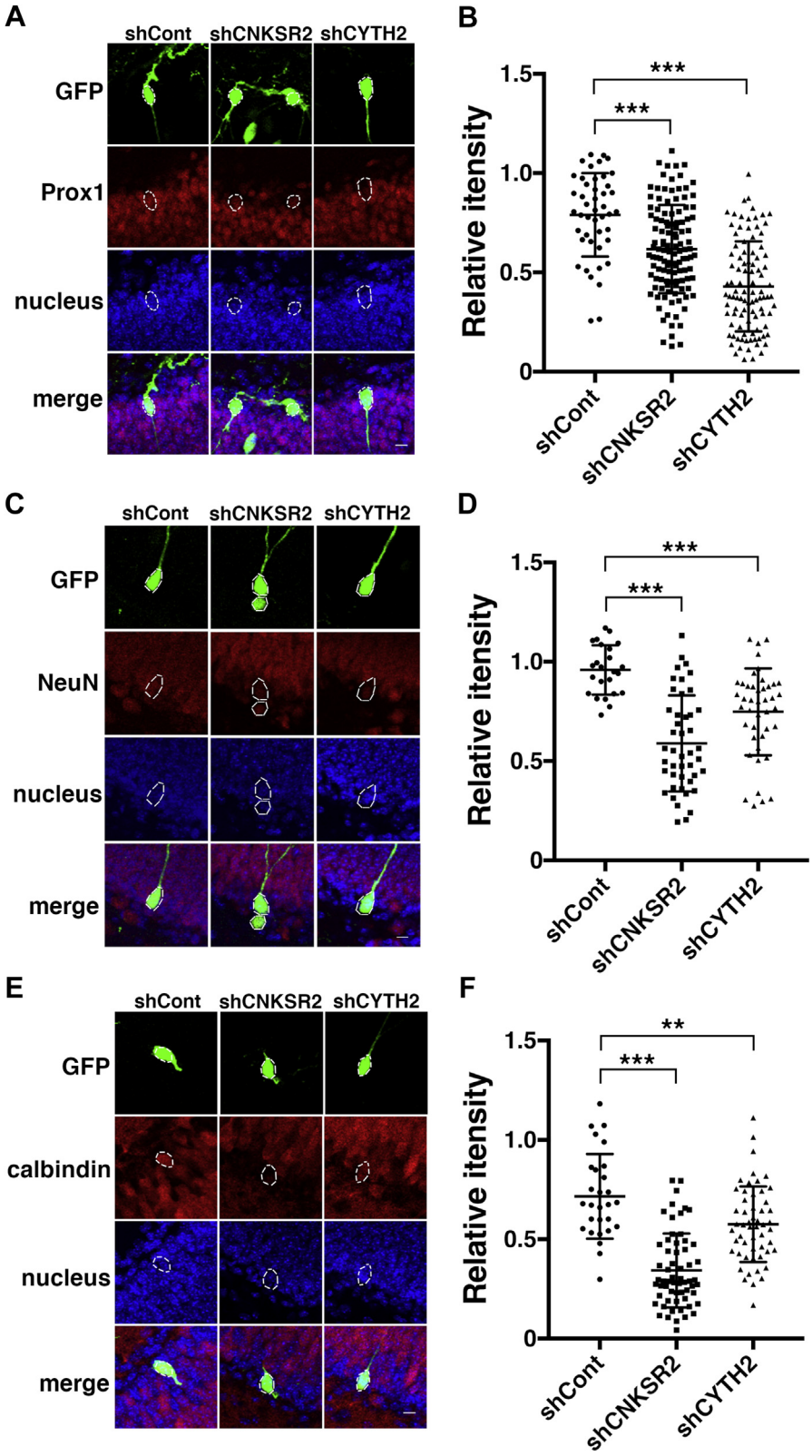

Figure 7. Effects of knockdown of CNKSR2 and CYTH2 on the differentiation of neonatally born dentate granule cells. *A*, immunohistochemical detection of Prox1. pCAG-GFP was coelectroporated with shCont, shCNKSR2#2, or shCYTH#2 into the lateral ventricle of P0 mice. After 21 days, coronal sections were prepared and stained with anti-GFP (*green*) and anti-Prox1 (*red*). Nuclei were stained with DAPI (*blue*). *B*, the intensity of Prox1 in *A* was quantified and graphed. Each bar shows mean ± SD. shCont, n = 45 form 15 animals; shCNKSR2, n = 119 from 11 animals; shCYTH2, n = 98 from ten animals. ***$p < 0.001$. *C*, expression of NeuN. Coronal sections prepared as in *A* were stained for GFP (*green*), NeuN (*red*), and nuclei (*blue*). *D*, the intensity of NeuN in *C* was quantified and graphed as in *B*. Each bar shows mean ± SD. shCont, n = 24 cells from nine animals; shCNKSR2, n = 45 cells from nine animals; shCYTH2, n = 43 cells from nine animals. ***$p < 0.001$. *E*, expression of calbindin. Coronal sections prepared as in *A* were stained for GFP (*green*), calbindin

The biological significance of CNKSR2 stabilization by protein partners is unclear, despite the implications of this molecular phenomenon on cellular homeostasis and regulation of tissue growth. For example, Smurf2, a HECT E3 ubiquitin ligase, has been reported to bind and stabilize CNKSR2 in breast cancer cells (32, 33). However, the roles for CNKSR2 and their binding partners in neurons are poorly characterized. However, given that Smurf2 WW2 domain binds to an "SPPPPY" motif at 702–707 amino acid sequence in CNKSR2 and forms an energy stable complex (32), while the N-terminal coiled-coil domain of CYTH2 interacts with the C-terminal region of CNKSR2 (aa 907–990) (22), it would seem that the C-terminal (aa700–990) region of CNKSR2 is essential for its ubiquitin-proteasome-mediated degradation. Indeed, four putative sites (K932, K959, K963, and K974) for CNKSR2 within aa907–aa990 are predicted as the ubiquitination sites (BDM-PUB, http://bdmpub.biocuckoo.org/index.php).

Mutations of *CNKSR2* have been identified in individuals diagnosed with ID and seizures (13–19). As the hippocampus is critical to the brain's functions, including learning and memory, disruptions to genes that influence hippocampal development would be relevant to human mental health and dysfunction. We found that suppression of CNKSR2 during the development in P0 hippocampal granule neurons resulted in their ectopic localization and their abnormal maturation within the P21 hippocampus. Indeed, suppression of CNKSR2 also disrupted the expression of markers of granule cell differentiation, including Prox1, NeuN, and the mature neuron marker calbindin. These findings with cells within rodent brains raise the possibility that inactivating mutations to *CNKSR2* may result in defective hippocampal development in humans, leading to brain disorders (34).

We found that the disruption of a CNKSR2-interacting protein CYTH2, but not ARHGAP39, caused developmental deficits of dentate granule cells, although both of these molecules increased the stability of CNK2. CYTH2 is characterized as a GEF for ARF small GTPases (35) to activate Rac signaling, while ARHGAP39, a GAP for Rac and Cdc42, serves as a negative regulator for Rac (36). It is noteworthy that Rac and Cdc42 are essential to hippocampal development (30), and their functional deficits are implicated in neurodevelopmental disorders (37–42). CYTH2 and ARHGAP39 both stabilize CNKSR2 expression yet play distinct roles in dentate granule cell development.

Prox1 and calbindin are dentate granule cell markers; the former is expressed in many cells during differentiation, while the latter is limited in the late maturation phase (43). Knockdown of CNKSR2 and CYTH2 led to a reduction in immunodetectable Prox1 and calbindin signals in cells that were abnormally localized to the GCL/hilus border or the hilus. These results demonstrate that CNKSR2 and CYTH2 are relevant to dentate granule cell differentiation, including the polarity, migration, and localization of these neonatally born P0 granule cells. In conclusion, we clarified the new role of CNKSR2 in the development of dentate gyrus *in vivo*. This finding may contribute to understanding the molecular mechanism of neonatal dentate gyrus development and to revealing the pathophysiology of neurodevelopmental disorders with the *CNKSR2* gene abnormalities.

Experimental procedures

Ethics statement

We adhere to the Fundamental Guidelines for Proper Conduct of Animal Experiments and Related Activity in Academic Research Institution under the jurisdiction of the Ministry of Education, Culture, Sports, Science and Technology, Japan. All protocols for animal handling and treatment were reviewed and approved by the Animal Care and Use Committee of Institute for Developmental Research, Aichi Developmental Disability Center (approval number; 2019-013).

Plasmid construction

Mouse cDNAs of CNKSR2, CYTH2, ARHGAP39, and ARHGEF7 were amplified by PCR with an E16 mouse brain RNA pool and cloned into pCAG-MCS2-myc, pCAG-MCS2-Flag, and pCAG-MCS2-GFP vectors (44). A GFP-expression plasmid, pCAG-GFP, was a gift from Dr Connie Cepko (Addgene plasmid # 11150) (45). For RNA interference, the following target sequences were inserted to pSUPER-puro vector (OligoEngine); luciferase (negative control), CGTAC GCGGAATACTTCGA (155–173) (46); CNKSR2, GAATTA TGGCTTAGAAACA (228–246, CNKSR2#1) and GTATAT GAAACTGAAAATA (529–547, CNKSR2#2); CYTH2, GCTTTACATTCCCAACAAT (972–990, CYTH2#1) and GAAGAAGAAGCAAGAACAA (1179–1197, CYTH2#2); ARHGAP39, GCTCTTTGACCCCAATACA (219–237, ARHGAP39#1) and AAGCTAATCCAAATGTAT (2227–2244, ARHGAP39#2). Numbers indicate the positions from translational start sites. We named these vectors as shCont, shCNKSR2#1 and #2, shCYTH2#1 and #2, shARHGAP39#1 and #2, and used for RNAi experiments. To generate RNAi-resistant CNKSR2, CNKSR2R, silent mutations were introduced in the target sequence of CNKSR2#2 as underlined (GTTTACGAGACAGAGAACA).

Antibodies

Recombinant fragment (aa 651–850) of CNKSR2 was produced in *E. coli* with pGS21a vector (GenScript Japan) and used as an antigen. A rabbit polyclonal antibody (anti-CNKSR2) was generated and affinity-purified on a column where the antigen had been conjugated. Polyclonal anti-GFP (Medical & Biological Laboratories), anti-calbindin (47), anti-Prox1 (Millipore), anti-NeuN (Millipore), and anti-CYTH2 (Proteintech) were used as primary antibodies. Mouse monoclonal anti-myc (Medical & Biological Laboratories) and rat

(*red*), and nuclei (*blue*). *F*, the intensity of calbindin shown in *E* was quantified and graphed as in *B*. Each bar shows mean ± SD. shCont, n = 28 from nine animals; shCNKSR2, n = 61 from ten animals; n = 54 from ten animals. ***$p < 0.001$, **$p < 0.01$. Scale bars, 10 μm. Images were captured with FV1000 confocal microscope.

monoclonal anti-GFP (Nacalai Tesque) were also used. CF488A conjugated anti-rabbit IgG and CF543 conjugated anti-mouse IgG (Biotinum Co) were used as secondary antibodies.

Cell culture, transfection, and preparation of cell extracts

COS7 and Neuro2a cells were cultured as described (48). Transient transfection was carried out using polyethyleneimine MAX reagent (Polysciences). After 24–48 h of transfection, cells were collected with the 50 mM Tris-HCl buffer, pH 7.5, containing 2% SDS, 0.1 M NaF, 5 mM EDTA, and protease inhibitor cocktail (Nacalai Tesque) (lysis buffer). Each suspension was sonicated at 0 °C for 1 min and centrifuged at 10,000*g* for 10 min at 4 °C. The supernatants were used as total cell extracts. Protein concentration was determined using bovine serum albumin as the standard using a micro bicinchoninic acid protein assay kit (Thermo Scientific). To select CNKSR2-deficient Neuro2a cells, cells were transfected with EGFP-C1 (Clontech Laboratories) and the knockdown vector. After 48 h, cells were treated with 600 μg/ml G418 (Sigma) for 48 h.

Immunoprecipitation

Immunoprecipitation was done as previously described (49). Briefly, COS7 cells transiently expressing various tagged proteins were extracted with immunoprecipitation (IP) buffer containing 50 mM Tris-HCl (pH 7.5), 150 mM NaCl, 1 % NP-40, 1 mM Na_3VO_4, and protease inhibitor cocktail (Nacalai Tesque). For the immunoprecipitation of endogenously expressed CNKSR2, the cerebral cortex and hippocampus dissected from mice at 7 months were homogenized with IP buffer. Insoluble materials were removed by centrifugation at 10,000*g* at 4 °C for 10 min. Resultant supernatants were incubated with the appropriate antibody at 4 °C for 1 h, added protein A sepharose beads, and incubated for an additional 1 h. In some experiments, we also used Protein A Mag Sepharose (Cytiva). The precipitates were subjected to SDS-PAGE followed by western blotting. Immunoreactive bands were visualized by the C-DiGit chemiluminescence western blot scanner (LI-COR).

Preparation of extracts from mouse brain for western blotting

Brains were dissected from mice at various stages and prepared extracts as previously described (50). Briefly, tissues were homogenized with the lysis buffer, sonicated at 0 °C for 1 min, and centrifuged at 125,000*g* for 20 min at 4 °C. The supernatants were used as whole tissue extracts. Protein concentration determination and western blotting were carried out as described above.

Immunohistochemistry

Mice were transcardially perfused with 4% paraformaldehyde in phosphate-buffered saline (PBS). Fixed brains were embedded in paraffin and cut into sub serial coronal sections (6-μm thickness) at the level of the dorsal hippocampus. After deparaffinization, sections were treated with citric acid and then processed for immunohistochemistry as reported previously (48). Images were obtained using a BZ-9000 microscope (Keyence).

In vivo *electroporation into the hippocampus of neonatal mice and immunostaining*

In vivo electroporation into neonatal mice was performed with the previously published method (25). In brief, 1 μl of DNA solution was injected into the lateral ventricle of postnatal day 0 (P0) mice. Successfully injected pups were immediately electroporated with a tweezers-type electrode (CUY650P5, Nepa Gene) using NEPA21 or CUY21 device (Nepa Gene). Five pulses of 100 V were given of 50 msec duration with a 950 msec interval, and electroporated animals were returned to their dam. After indicated days, animals were transcardially perfused with 4% paraformaldehyde in PBS. Brains were then dissected and placed at 4 °C for overnight in the same solution, washed with PBS, and mounted in 3% agarose in PBS. Sections (70 μm- or 100 μm-thickness) were cut using the HM 650 V vibrating-blade microtome (Thermo Scientific). Immunostaining was performed with free-floating sections (30). To quantify GFP-labeled cells in the dentate gyrus, we usually prepared serial brain sections containing dentate gyrus (100 μm-thickness), picked one slice from every three slices (six slices in total), stained for GFP, and quantified. For the quantitation of the localization of cells, we used z-stacked images captured by a fluorescent microscope (BZ-9000; Keyence). For the quantitation of the expression of differentiation markers, we used images captured by a confocal laser microscope (FV1000, Olympus). For the morphological analyses, we presented z-stacked images captured by FV1000. Image analyses were performed with ImageJ (US National Institutes of Health; https://imagej.nih.gov/). As for the quantitation of the distribution of GFP-positive cells in brain slices at P4, GFP-signal intensity in distinct regions (bin 1–4) was measured by ImageJ software. Relative fluorescence intensities in each bin to total fluorescence intensities were calculated.

Statistical analysis

Statistical analyses were GraphPad PRISM (GraphPad Software). Comparisons between the two groups were performed by *t* test (Fig. 1*C*). For other experiments, we analyzed data by one-way ANOVA with a post-hoc Dunnett's test (Figs. 1*E*, 4, *Bf* and *Cf*, and 7) or two-way ANOVA with a post-hoc Dunnett's test (Figs. 4, *Be* and *Ce*, 5*B* and S3) or Tukey test (Fig. S2).

Data availability

All data are contained within the manuscript.

Supporting information—This article contains supporting information.

Acknowledgments:—We thank Prof. Julian Heng (Curtin University, Perth, Australia) for the language editing of the manuscript. We

thank Ms Noriko Kawamura for her technical assistance. This work was supported in part by JSPS KAKENHI Grant (grant no. 16K08264 and 19K07059) and a grant-in-aid of Takeda Science Foundation.

Author contributions—H. I. conceptualization; H. I. data curation; H. I. formal analysis; H. I. funding acquisition; H. I., R. M., M. Noda , T. I., and M. Nishikawa investigation; H. I. methodology; H. I. project administration; H. I. resources; H. I. and K.-i. N. supervision; H. I. validation; H. I. writing–original draft; H. I. and K.-i. N. writing–review and editing.

Conflict of interest—The authors declare that they have no conflict of interest with the content of this article.

Abbreviations—The abbreviations used are: GAP, GTPase-activating protein; GEF, guanine nucleotide exchange factor; ID, intellectual disability; IP, immunoprecipitation; GCL, granule cell layer.

References

1. Sontheimer, H. (2015) Chapter 11 - Neurodevelopmental disorders. In: Sontheimer, H., ed. *Diseases of the Nervous System*, Academic Press, San Diego, CA: 319–347
2. Li, Y., Shen, M., Stockton, M. E., and Zhao, X. (2019) Hippocampal deficits in neurodevelopmental disorders. *Neurobiol. Learn. Mem.* **165**, 106945
3. Bayer, S. A. (1980) Development of the hippocampal region in the rat I. Neurogenesis examined with 3H-thymidine autoradiography. *J. Comp. Neurol.* **190**, 87–114
4. Verkerk, A. J. M. H., Pieretti, M., Sutcliffe, J. S., Fu, Y. H., Kuhl, D. P. A., Pizzuti, A., Reiner, O., Richards, S., Victoria, M. F., Zhang, F., Eussen, B. E., van Ommen, G. J. B., Blonden, L. A. J., Riggins, G. J., Chastain, J. L., *et al.* (1991) Identification of a gene (FMR-1) containing a CGG repeat coincident with a breakpoint cluster region exhibiting length variation in fragile X syndrome. *Cell* **65**, 905–914
5. Pieretti, M., Zhang, F., Fu, Y. H., Warren, S. T., Oostra, B. A., Caskey, C. T., and Nelson, D. L. (1991) Absence of expression of the FMR-1 gene in fragile X syndrome. *Cell* **66**, 817–822
6. Ichtchenko, K., Nguyen, T., and Südhof, T. C. (1996) Structures, alternative splicing, and neurexin binding of multiple neuroligins. *J. Biol. Chem.* **271**, 2676–2682
7. Bhakar, A. L., Dölen, G., and Bear, M. F. (2012) The pathophysiology of fragile X (and what it teaches us about synapses). *Annu. Rev. Neurosci.* **35**, 417–443
8. Baudouin, S. J., Gaudias, J., Gerharz, S., Hatstatt, L., Zhou, K., Punnakkal, P., Tanaka, K. F., Spooren, W., Hen, R., De Zeeuw, C. I., Vogt, K., and Scheiffele, P. (2012) Shared synaptic pathophysiology in syndromic and nonsyndromic rodent models of autism. *Science* **338**, 128–132
9. Jamain, S., Quach, H., Betancur, C., Rastam, M., Colineaux, C., Gillberg, I. C., Soderstrom, H., Giros, B., Leboyer, M., Gillberg, C., and Bourgeron, T. (2003) Mutations of the X-linked genes encoding neuroligins NLGN3 and NLGN4 are associated with autism. *Nat. Genet.* **34**, 27–29
10. Yan, J., Oliveira, G., Coutinho, A., Yang, C., Feng, J., Katz, C., Sram, J., Bockholt, A., Jones, I. R., Craddock, N., Cook, E. H., Vicente, A., *et al.* Cook, E. H., Jr., Vicente, A., and Sommer, S. S. (2005) Analysis of the neuroligin 3 and 4 genes in autism and other neuropsychiatric patients. *Mol. Psychiatry* **10**, 329–332
11. Lubs, H. A., Stevenson, R. E., and Schwartz, C. E. (2012) Fragile X and X-linked intellectual disability: Four decades of discovery. *Am. J. Hum. Genet.* **90**, 579–590
12. Tejada, M. I., and Ibarluzea, N. (2020) Non-syndromic X linked intellectual disability: Current knowledge in light of the recent advances in molecular and functional studies. *Clin. Genet.* **97**, 677–687
13. Aypar, U., Wirrell, E. C., and Hoppman, N. L. (2015) CNKSR2 deletions: A novel cause of X-linked intellectual disability and seizures. *Am. J. Med. Genet. A* **167**, 1668–1670
14. Damiano, J. A., Burgess, R., Kivity, S., Lerman-Sagie, T., Afawi, Z., Scheffer, I. E., Berkovic, S. F., and Hildebrand, M. S. (2017) Frequency of CNKSR2 mutation in the X-linked epilepsy-aphasia spectrum. *Epilepsia* **58**, e40–e43
15. Houge, G., Rasmussen, I. H., and Hovland, R. (2012) Loss-of-function CNKSR2 mutation is a likely cause of non-syndromic X-linked intellectual disability. *Mol. Syndromol.* **2**, 60–63
16. Hu, H., Haas, S. A., Chelly, J., Van Esch, H., Raynaud, M., de Brouwer, A. P., Weinert, S., Froyen, G., Frints, S. G., Laumonnier, F., Zemojtel, T., Love, M. I., Richard, H., Emde, A. K., Bienek, M., *et al.* (2016) X-exome sequencing of 405 unresolved families identifies seven novel intellectual disability genes. *Mol. Psychiatry* **21**, 133–148
17. Polla, D. L., Saunders, H. R., Vries, B. B. A., Bokhoven, H., Brouwer, A. P. M., de Vries, B. B. A., van Bokhoven, H., and de Brouwer, A. P. M. (2019) A de novo variant in the X-linked gene CNKSR2 is associated with seizures and mild intellectual disability in a female patient. *Mol. Genet. Genomic Med.* **7**, e00861
18. Sun, Y., Liu, Y. D., Xu, Z. F., Kong, Q. X., and Wang, Y. L. (2018) CNKSR2 mutation causes the X-linked epilepsy-aphasia syndrome: A case report and review of literature. *World J. Clin. Cases.* **6**, 570–576
19. Vaags, A. K., Bowdin, S., Smith, M. L., Gilbert-Dussardier, B., Brocke-Holmefjord, K. S., Sinopoli, K., Gilles, C., Haaland, T. B., Vincent-Delorme, C., Lagrue, E., Harbuz, R., Walker, S., Marshall, C. R., Houge, G., Kalscheuer, V. M., *et al.* (2014) Absent CNKSR2 causes seizures and intellectual, attention, and language deficits. *Ann. Neurol.* **76**, 758–764
20. Yao, I., Hata, Y., Ide, N., Hirao, K., Deguchi, M., Nishioka, H., Mizoguchi, A., and Takai, Y. (1999) MAGUIN, a novel neuronal membrane-associated guanylate kinase-interacting protein. *J. Biol. Chem.* **274**, 11889–11896
21. Lanigan, T. M., Liu, A., Huang, Y. Z., Mei, L., Margolis, B., and Guan, K. L. (2003) Human homologue of Drosophila CNK interacts with Ras effector proteins Raf and Rlf. *FASEB J.* **17**, 2048–2060
22. Lim, J., Ritt, D. A., Zhou, M., and Morrison, D. K. (2014) The CNK2 scaffold interacts with vilse and modulates Rac cycling during spine morphogenesis in hippocampal neurons. *Curr. Biol.* **24**, 786–792
23. Santy, L. C., and Casanova, J. E. (2001) Activation of ARF6 by ARNO stimulates epithelial cell migration through downstream activation of both Rac1 and phospholipase D. *J. Cell Biol.* **154**, 599–610
24. Bumeister, R., Rosse, C., Anselmo, A., Camonis, J., and White, M. A. (2004) CNK2 couples NGF signal propagation to multiple regulatory cascades driving cell differentiation. *Curr. Biol.* **14**, 439–445
25. Ito, H., Morishita, R., Iwamoto, I., and Nagata, K. (2014) Establishment of an *in vivo* electroporation method into postnatal newborn neurons in the dentate gyrus. *Hippocampus* **24**, 1449–1457
26. Frank, S. R., Hatfield, J. C., and Casanova, J. E. (1998) Remodeling of the actin cytoskeleton is coordinately regulated by protein kinase C and the ADP-ribosylation factor nucleotide exchange factor ARNO. *Mol. Biol. Cell.* **9**, 3133–3146
27. Srinivasaraghavan, K., Nacro, K., Grüber, G., and Verma, C. S. (2013) Effect of Ser392 phosphorylation on the structure and dynamics of the polybasic domain of ADP ribosylation factor nucleotide site opener protein: A molecular simulation study. *Biochemistry* **52**, 7339–7349
28. Van Den Bosch, M. T. J., Poole, A. W., and Hers, I. (2014) Cytohesin-2 phosphorylation by protein kinase C relieves the constitutive suppression of platelet dense granule secretion by ADP-ribosylation factor 6. *J. Thromb. Haemost.* **12**, 726–735
29. Anastasi, S., Zhu, S.-J., Ballarò, C., Manca, S., Lamberti, D., Wang, L.-J., Alemà, S., Yun, C.-H., and Segatto, O. (2016) Lack of evidence that CYTH2/ARNO functions as a direct intracellular EGFR activator. *Cell* **165**, 1031–1034
30. Ito, H., Morishita, R., Mizuno, M., Tabata, H., and Nagata, K. I. (2019) Rho family GTPases, Rac and Cdc42, control the localization of neonatal dentate granule cells during brain development. *Hippocampus* **29**, 569–578

31. Nicola, Z., Fabel, K., and Kempermann, G. (2015) Development of the adult neurogenic niche in the hippocampus of mice. *Front. Neuroanat.* **9**, 53
32. David, D., Jagadeeshan, S., Hariharan, R., Nair, A. S., and Pillai, R. M. (2014) Smurf2 E3 ubiquitin ligase modulates proliferation and invasiveness of breast cancer cells in a CNKSR2 dependent manner. *Cell Div.* **9**, 1–18
33. David, D., Surendran, A., Thulaseedharan, J. V., and Nair, A. S. (2018) Regulation of CNKSR2 protein stability by the HECT E3 ubiquitin ligase Smurf2, and its role in breast cancer progression. *BMC Cancer* **18**, 1–19
34. Scharfman, H., Goodman, J., and McCloskey, D. (2007) Ectopic granule cells of the rat dentate gyrus. *Dev. Neurosci.* **29**, 14–27
35. Chardin, P., Paris, S., Antonny, B., Robineau, S., Béraud-Dufour, S., Jackson, C. L., and Chabre, M. (1996) A human exchange factor for ARF contains Sec7- and pleckstrin-homology domains. *Nature* **384**, 481–484
36. Lundström, A., Gallio, M., Englund, C., Steneberg, P., Hemphälä, J., Aspenström, P., Keleman, K., Falileeva, L., Dickson, B. J., and Samakovlis, C. (2004) Vilse, a conserved Rac/Cdc42 GAP mediating Robo repulsion in tracheal cells and axons. *Genes Dev.* **18**, 2161–2171
37. Hiraide, T., Kaba Yasui, H., Kato, M., Nakashima, M., and Saitsu, H. (2019) A de novo variant in RAC3 causes severe global developmental delay and a middle interhemispheric variant of holoprosencephaly. *J. Hum. Genet.* **64**, 1127–1132
38. Costain, G., Callewaert, B., Gabriel, H., Tan, T. Y., Walker, S., Christodoulou, J., Lazar, T., Menten, B., Orkin, J., Sadedin, S., Snell, M., Vanlander, A., Vergult, S., White, S. M., Scherer, S. W., *et al.* (2019) De novo missense variants in RAC3 cause a novel neurodevelopmental syndrome. *Genet. Med.* **21**, 1021–1026
39. Motokawa, M., Watanabe, S., Nakatomi, A., Kondoh, T., Matsumoto, T., Morifuji, K., Sawada, H., Nishimura, T., Nunoi, H., Yoshiura, K. I., Moriuchi, H., and Dateki, S. (2018) A hot-spot mutation in CDC42 (p. Tyr64Cys) and novel phenotypes in the third patient with Takenouchi-Kosaki syndrome. *J. Hum. Genet.* **63**, 387–390
40. Martinelli, S., Krumbach, O. H. F. F., Pantaleoni, F., Coppola, S., Amin, E., Pannone, L., Nouri, K., Farina, L., Dvorsky, R., Lepri, F., Buchholzer, M., Konopatzki, R., Walsh, L., Payne, K., Pierpont, M. E., *et al.* (2018) Functional dysregulation of CDC42 causes diverse developmental phenotypes. *Am. J. Hum. Genet.* **102**, 309–320
41. Reijnders, M. R. F., Ansor, N. M., Kousi, M., Yue, W. W., Tan, P. L., Clarkson, K., Clayton-Smith, J., Corning, K., Jones, J. R., Lam, W. W. K., Mancini, G. M. S., Marcelis, C., Mohammed, S., Pfundt, R., Roifman, M., *et al.* (2017) RAC1 missense mutations in developmental disorders with diverse phenotypes. *Am. J. Hum. Genet.* **101**, 466–477
42. Takenouchi, T., Kosaki, R., Niizuma, T., Hata, K., and Kosaki, K. (2015) Macrothrombocytopenia and developmental delay with a de novo CDC42 mutation: Yet another locus for thrombocytopenia and developmental delay. *Am. J. Med. Genet. A* **167A**, 2822–2825
43. Kempermann, G., Song, H., and Gage, F. H. (2015) Neurogenesis in the adult hippocampus. *Cold Spring Harb. Perspect. Biol.* **7**, a018812
44. Ito, H., Morishita, R., Shinoda, T., Iwamoto, I., Sudo, K., Okamoto, K. I., and Nagata, K. (2010) Dysbindin-1, WAVE2 and Abi-1 form a complex that regulates dendritic spine formation. *Mol. Psychiatry* **15**, 976–986
45. Matsuda, T., and Cepko, C. L. (2007) Controlled expression of transgenes introduced by *in vivo* electroporation. *Proc. Natl. Acad. Sci. U. S. A.* **104**, 1027–1032
46. Bot, I., Guo, J., Van Eck, M., Van Santbrink, P. J., Groot, P. H., Hildebrand, R. B., Seppen, J., Van Berkel, T. J., and Biessen, E. A. (2005) Lentiviral shRNA silencing of murine bone marrow cell CCR2 leads to persistent knockdown of CCR2 function *in vivo*. *Blood* **106**, 1147–1153
47. Kurobe, N., Inaguma, Y., Shinohara, H., Semba, R., Inagaki, T., and Kato, K. (1992) Developmental and age-dependent changes of 28-kDa calbindin-D in the central nervous tissue determined with a sensitive immunoassay method. *J. Neurochem.* **58**, 128–134
48. Ito, H., Morishita, R., Sudo, K., Nishimura, Y. V., Inaguma, Y., Iwamoto, I., and Nagata, K.-I. (2012) Biochemical and morphological characterization of MAGI-1 in neuronal tissue. *J. Neurosci. Res.* **90**, 1776–1781
49. Ito, H., Morishita, R., and Nagata, K. (2016) Schizophrenia susceptibility gene product dysbindin-1 regulates the homeostasis of cyclin D1. *Biochim. Biophys. Acta* **1862**, 1383–1391
50. Ito, H., Morishita, R., Mizuno, M., Kawamura, N., Tabata, H., and Nagata, K. I. (2018) Biochemical and morphological characterization of a neurodevelopmental disorder-related mono-ADP-ribosylhydrolase, MACRO domain containing 2. *Dev. Neurosci.* **40**, 278–287